CHAPTER 88

Wave impact forces on mixed breakwaters

Stéphan T. Grilli [1], M. ASCE, Miguel A. Losada[2], and Francisco Martin [2]

Abstract : Flat impact of a solitary wave on a mixed breakwaters is experimentally and numerically studied, using a 2D nonlinear potential flow model. Free surface profiles, internal velocities, instantaneous pressure and pressure envelope on the wall, and on the berm, are analyzed based on both measurements and calculations. Results show, a converging flow occurs above the berm, followed by a small vertical jet, with large acceleration, that is responsible for large impact pressure on the wall. Short duration peak pressures occur above SWL, and quite large pressures also occur on the berm, as far away as twice the local depth from the wall. Maximum pressure force and overturning moment on the wall reach up to 9 and 15 times corresponding hydrostatic values based on water elevation at the wall.

Introduction

Mixed breakwaters are made of the combination of a vertical wall and a rubble mound berm (Fig. 1). Under wave action, they function as vertical walls during high tide, and as mound breakwaters during low tide. The design of mixed breakwaters requires that their upper part be safe against sliding and overturning due to wave impact pressure. Laboratory and field experiments show, impacts of normally incident breaking waves are the most severe (Goda, 1985). Geometrical parameters of the breakwater, such as berm depth, $d = h - h_1$, and length, in water of depth h (Fig. 1), control conditions under which impulsive breaking of incident waves of height H can occur on the wall.

Extensive experimental work was carried out over the past 50 years for the evaluation of the peak pressure on vertical seawalls. Results were analyzed mostly based on Bagnold's simple theory (Goda 1985). Kirkgöz 1991 (KIR), in his recent review of this experimental work, shows that the average maximum pressure on vertical walls, p_{max}, varies between 20 and 75 times $\rho g H$ (where ρ is the water density, and g the acceleration of gravity), and that the highest maximum pressure can reach up to 220 times this value. Variations in maximum pressure depend on the incident wave type (periodic, solitary) and characteristics, on the experimental scale, and on the type and location of measuring devices. In addition, maximum

[1]Assistant Professor, Department of Ocean Engineering, University of Rhode Island, Kingston, RI 02881, USA, Ph.Nb.: (401) 792-2550

[2]Professor and Graduate Student, Departamento de Ciencias y Tecnicas del Agua y del Medio Ambiente, University of Cantabria, Santander 39005, Spain

pressures on the wall vary with the bottom slope in front of the wall. Kirkgöz 1982, based on laboratory experiments, showed that greatest impact pressures are obtained with a 1/10 slope in front of the wall. KIR also showed that largest impact pressures are obtained for an inclined wall, with a 10° to 20° backward slope with respect to the vertical. Finally, as far as scale effects are concerned, Führböter 1985 showed that experimental pressures obtained in small-scale tests are larger than prototype pressures, due to increasing aeration effects at larger scale.

In the same line, Partenscky 1988 showed, based on laboratory experiments with mixed breakwaters, that highest pressures are exerted on the wall when the colliding wave has an almost vertical face. In this case, the maximum impact force on the wall, F_x, can rise to more than 10 times the hydrostatic force, $F_{Hx} = \frac{1}{2}\rho g(d+\eta)^2$, based on wave elevation η at the wall.

In the experimental studies reported above, results were mostly analyzed, using statistical theories and semi-empirical methods. Few viable theoretical approaches indeed exist that can model waves close to breaking over an arbitrary bottom and structure geometry, and thus be used to analyze the magnitude of impact pressures as a function of the detailed incident wave flow. In fact, only two theoretical approaches have been developed so far, that have been successfully applied to calculating wave impact on vertical walls : (i) Solution of two-dimensional (2D) fully nonlinear potential flow equations, using a Boundary Integral Equation method (BIE) (e.g., Cooker and Peregrine 1991 (CP)); (ii) Solution of 2D Euler equations, using a Volume Of Fluid method (VOF) (e.g., Wang and Su 1992). The first method turns out to be very efficient and accurate in dealing with this problem, but is limited to prior to wave breaking first occurs. The second method is less accurate but is somewhat more efficient in dealing with wave breaking and discontinuities. Experimental results for wave impact on the wall can be classified into three types, that must be considered when developing theoretical or numerical models : (i) Non-breaking waves; (ii) Waves with flat impact on the wall (i.e., with an almost vertical front face); (iii) Waves with falling breaking jets, and imprisoned air under the wave (e.g., plunging breaker). Models based on satisfying continuity equation in the fluid, like the BIE method, can deal with cases (i) and (ii), in which very little or no air entrainment occurs, but they cannot deal with case (iii), further than the time the breaking jet impinges on the wall.

Experiments and calculations with non-breaking waves (case (i)) do not show occurrence of large impact pressures on the wall. The wave pressure and total wave force, instead, gently increase following the same pattern as wave runup on the wall. For sufficiently large incident waves, however, more complex pressure variations can be obtained, in the form of two successive pressure maxima, slightly before, and slightly after the time of maximum runup (see, results by Grilli and Svendsen 1991ab, using a BIE model and solitary waves). This double maximum is also supported by experiments. For flat impact of long waves on a vertical wall (case (ii)), calculations by CP confirmed experimental observations. Results showed, a maximum impact pressure of up to $60\rho gd$ occurs at the wall, while a vertical jet starts forming, with

vertical velocity and acceleration of up to $20\sqrt{gd}$ and $8000g$, respectively. CP also found, water compressibility does not play an important role in the process, provided no air is entrained, but suggested, wall and free surface roughness (not included in the calculations) are likely to be significant in reducing theoretical maximum pressures.

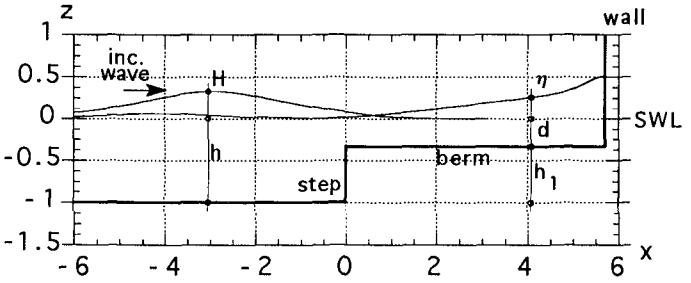

Figure 1: Sketch of a mixed breakwater, and main geometrical parameters.

In the present study, laboratory experiments are performed to measure wave impact pressure on the vertical wall of a mixed breakwater, in a similar case (ii) as above, for which incident wave front face is almost vertical at the time of impact, and there is no or very little air entrainment. Solitary waves are used as incident waves, both for simplicity, and because they are believed to have the largest impulse, impact force and runup on structures. They also represent a simplified tsunami model. Experimental results are compared with computational results obtained using the 2D fully nonlinear BIE potential model by Grilli *et al.* 1989, 1990 (GSS). Largest impact pressures on the wall are obtained for incident waves with large height to depth ratios. This was achieved in the calculations by CP, by introducing very high but quite arbitrary long waves into their model. Wave propagation over a flat bottom and impact on a vertical wall were then calculated. The present numerical model works for arbitrary geometry and incident wave conditions. Hence, this enables us to closely reproduce the experimental set-up in the numerical model (Fig. 2a), while studying a more realistic coastal structure.

Laboratory experiments

Experiments are conducted in the 70x2x2m wave flume of the University of Cantabria. Solitary waves are generated using a computer-controlled hydraulic piston wavemaker, at one extremity of the flume. The wave generation method is similar to that of Goring 1978. The flume width is divided into two subsections, the smallest one, in which a plywood step is built on the bottom, being 0.9m wide. A vertical plate is fixed above the step, to complete the mixed breakwater. The distance from the wavemaker paddle to the breakwater step is approximately 45m. The step height is h_1 =20cm, and the water depth in the flume is adjusted to h =30cm, so that the step aspect ratio is $h_1' = 0.667$ (primes denote nondimensional variables : length is divided by depth

h, time by $\sqrt{\frac{h}{g}}$, and celerity by $\sqrt{gh}$). The experimental set-up is illustrated in Figure 1.

A solitary wave is generated by the wavemaker at $150h$ from the step, and propagates down the flume. The incident wave profile modifies its shape while propagating down the tank, mostly due to higher-order nonlinear effects not included in Goring's first-order solution (Grilli & Svendsen 1991b). The incident wave eventually stabilizes in the form of a slightly smaller solitary wave, after $80h$ or so of propagation. Side-wall and bottom friction also lead to a small decrease in wave height. This was studied by Losada *et al.* 1989 (LVM), who found the decrease to be almost negligible when all tank surfaces are maintained smooth enough. To eliminate both of these (frictionless and friction) effects of amplitude reduction from the experimental results and thus make the comparison with the potential flow model more accurate, LVM measured incident wave height at a small distance in front of the bottom step. A similar procedure has been adopted in the present experiments, in which a solitary wave is generated in the tank, such that it has the heigth $H = 9.67$cm, or $H' = 0.322$, at $x' = -7$, where incident wave height is defined. Experiments are first realized without the vertical wall in the breakwater, thereby re-creating conditions of the study by LVM. In this case, the incident wave overturns over the step as a plunging breaker. The vertical wall is then added to the breakwater model and its horizontal position is adjusted to $x' = 5.69$, in order to make the incident wave impact the wall with an almost vertical front face. Hence, final length of the mixed breakwater berm is $5.69h$.

Water surface elevation is measured using wave gages placed at the tank centerline. Characteristics of the gages are : DHI capacitance gages type 202/60, with wave meter amplifiers 102/E (linearity better than 0.5%). Total water depth is recorded every 0.01s, over a period of about 10s for each experiment. Due to a limited number of gages (5), identical experiments are repeated several times, and gages, attached to a movable carriage, are moved to different locations until the full experimental region is covered. A one-gage overlap is maintained between successive repetitions, in order to check the repeatability of experiments. Experiments are discarded when differences in measured surface elevations are larger than 1.5mm, or 0.5% of the water depth, between two repetitions of an experiment. A very high degree of repeatability of experiments is found when applying this criterion, confirming the good control of all experimental procedures.

Flow velocities are recorded above the step, in front of the vertical wall, using a 6W LASER phase Doppler anemometer, Dantec 60x10 optical fibers, and a Dantec 58N20 particle dynamics analyzer. The positioning system is a Dantec 57H00 traversing system, that moves the optical fibers over a 2.5x2.5cm grid. The sampling frequency is variable, with burst detection (100-800Hz).

Dynamic pressure is measured using piezoelectric pressure gages that automatically eliminate hydrostatic pressure due to still water level (SWL). Corrected total pressure p is presented in the following. Characteristics of the gages are : transducer

type PDCR 830-201-Druck Limited, with strain amplifier DHI 106/E (linearity better than 0.1%), and the sampling frequency is 600Hz. Diameter of the pressure gages is about 15mm. The pressure is recorded at 11 locations along the vertical wall (Fig. 3), from $z' = -0.23$ to $z' = 0.77$, and at 9 locations on the berm (Fig. 3), from $x' = 4.69$ to $x' = 5.62$.

Experimental results are detailed in a following section.

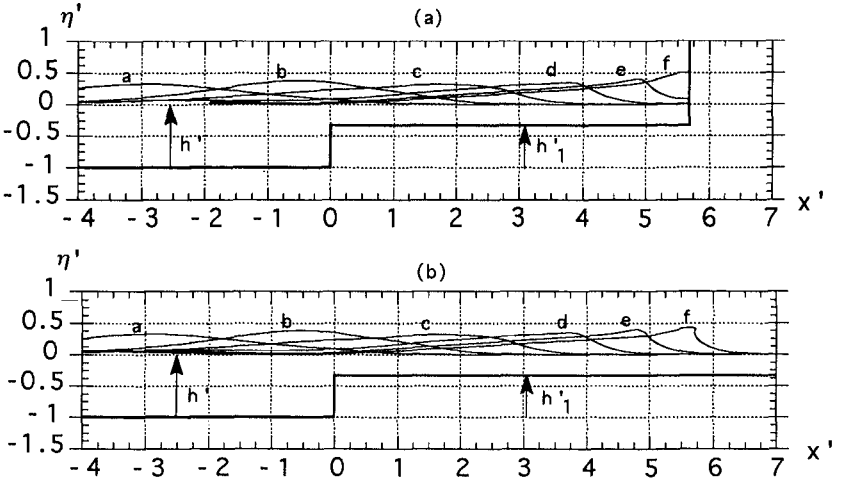

Figure 2: Computed surface elevations with $H' = 0.322$: (a) for the mixed breakwater, curves a-f, $t' = 3.46, 5.73, 7.55, 9.03.\ 10.10, 10.70$; (b) for the step in the bottom, curves a-f, $t' = 3.46, 5.70, 7.47, 8.93, 9.98, 10.77$.

Numerical experiments

The fully nonlinear 2D potential model by GSS, and its most recent extensions, are used in the numerical computations. In this model, continuity equation takes the form of a Laplace's equation, expressed in a BIE formulation discretized using a higher-order Boundary Element Method. Time integration is based on a second-order Taylor expansion, similar to that introduced by Dold & Peregrine 1986, expressed in a mixed Eulerian-Lagrangian representation. Both dynamics and kinematics free surface boundary conditions are exactly specified in the model, and no-flow conditions are prescribed along solid boundaries. Solitary waves are generated at the computational domain leftward boundary, as in laboratory experiments, by simulating a piston wavemaker motion according to Goring's 1978 procedure. It should be reminded, that computations based on potential flow theory are only valid up to the instant waves overturn and break, and that potential flow also implies, dissipations and flow separation cannot be modeled. Details of the numerical implementation can be found in GSS, along with a discussion of problems associated with surface piercing bodies such

as wavemakers. Details of the generation of solitary waves by a piston wavemaker are also given in Grilli & Svendsen 1990.

As already mentioned, computations closely reproduce the experimental set-up (Fig. 2a). To reduce computation time, however, the horizontal length of the computational domain in front of the berm ($x < 0$) is reduced to $20h$, versus $150h$ in the laboratory experiments. A solitary wave is generated in the model, and its initial height is adjusted in order to be $H' = 0.322$, at $x' = -7$, as in the experiments. The origin of time, $t' = 0$, for both experimental and numerieal results corresponds to the instant, the crest of the incident wave crosses the point $x' = -7$.

Numerical data are selected to ensure good accuracy of the results, considering both the domain geometry and the incident wave condition. The discretization uses 161 nodes on the free surface, and 160 spline boundary elements. Other boundaries are discretized using 3-node quadratic elements. The total number of nodes is 256, which leads to a computing time of about 3s per time step (IBM 3090/300, including saving and postprocessing of results). The initial distance between nodes on the free surface is $\Delta x' = 0.1606$. Time steps are automatically selected, as in Grilli & Svendsen 1990, to ensure optimal accuracy and stability of the computations (constant mesh Courant number condition, starting with $\Delta t' = 0.08$). The accuracy of the computations is checked by verifying conservation of wave mass above SWL, and total energy. With the selected numerical data, both of these stay constant to within 0.05% during most of the wave propagation. Slightly after maximum impact pressure occurs on the wall, however, a small jet starts forming at the wall (see next section), with very large vertical velocity and acceleration. Discretization nodes—identical to Lagrangian markers—tend to concentrate in this jet, and time step reduces accordingly. This makes numerical errors in wave mass and energy increase, and computations have to be stopped (shortly after the last surface profile shown in Fig. 2a). For the last computed wave profile, the time step has reduced to $\Delta t' = 0.0012$, and the numerical error on wave mass is 0.10%. Total number of time steps, however, is only about 300.

Computations with the step in the bottom and no vertical wall have also been made, using similar numerical data, to compare with the experimental procedure of selecting the position of the vertical wall in the mixed breakwater (Fig. 2b). Numerical results essentially agree with experiments. The incident wave overturns over the berm at $x' = 5.56$, with a local breaking index $\frac{H_b}{d} = 1.31$ (curve f in Fig. 2b). Details of these computations and related problems can be found in Grilli *et al.* 1992.

Numerical results with the mixed breakwater are detailed in the next section.

Results and discussions

Experimental and numerical results are presented and discussed in parallel in the following, for the case of Fig. 2a ($H' = 0.322$).

Free surface elevation.— Figure 2a shows computed free surface elevations up to

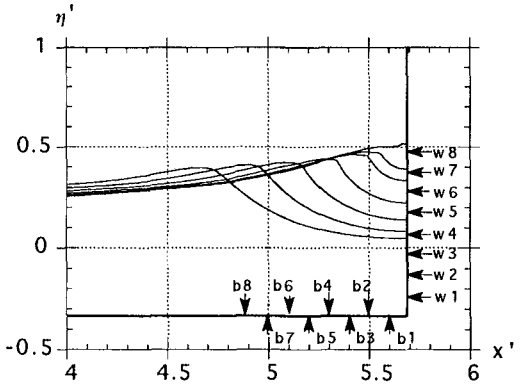

Figure 3: Blow-up of Fig. 2a, close to the wall (t' =9.88, 10.10, 10.30, 10.47, 10.60, 10.65, 10.70, left to right), with location of pressure sensors (b1-b8) and (w1-w8).

the instant of maximum impact pressure on the vertical wall ($t' = 10.70$), and Figure 3 shows a blow-up of these near the wall, over a period of 0.82 time unit.

Results in Fig. 2a show, wave height increases up to a maximum, $H'_{max} = 0.384$ (curve b), upstream of the step, and decreases downstream of the step, to $H'_{min} = 0.321$ (curve c). For larger x, wave height increases again, up to the instant of maximum impact on the wall. Computed free surface envelope is compared to measurements in Fig. 4. One sees, the agreement between both of these is quite good up to the step ($x' = 0$). Downstream of the step ($x' > 0$), the agreement is less good, and the model overpredicts maximum wave height by about 15%. This is due to energy loss by flow separation at the step, not included in the model (see LVM for detail).

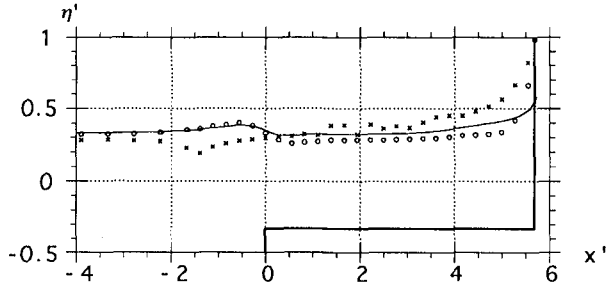

Figure 4: Free surface envelope of incident wave : (o) experimental; (—) numerical. Experimental envelope of reflected wave (×).

In Fig. 3, one also sees, a small jet starts forming close to the wall, in the last surface profile. Maximum water velocity and acceleration in the jet reach about

$20\sqrt{gd}$ and $9800g$, respectively, at this stage. These large values are similar to those obtained by CP, and provide a physical justification for the occurrence of large impact pressure on the wall. The internal velocity field (discussed in the next section) indeed shows, the wave flow strongly converges, in a jet-like manner, towards the upper part of the wall, while its horizontal momentum gradually transforms into vertical acceleration. This acceleration, in turn, is balanced by a large pressure gradient close to the wall (as can be seen from Euler equations).

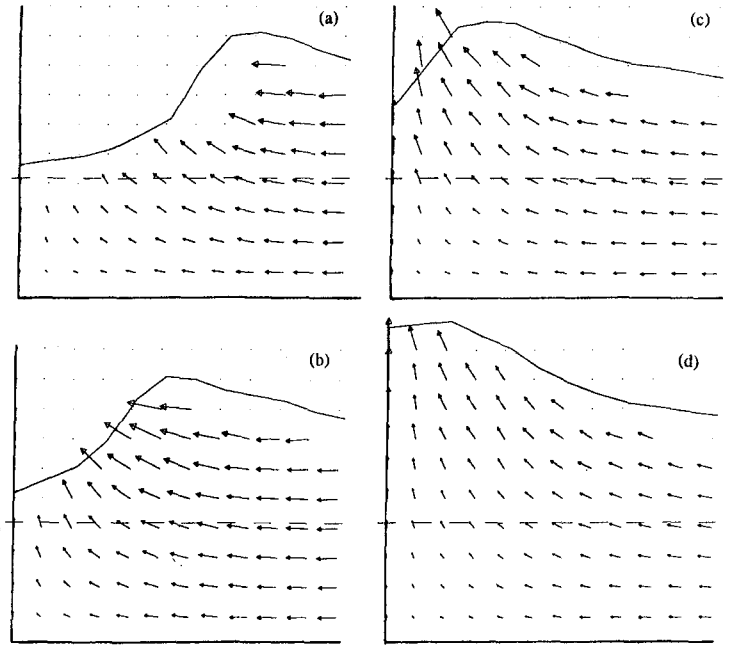

Figure 5: Internal velocity field at $t' =$: (a) 9.25; (b) 9.75; (c) 10.25; (d) 10.75.

Internal flow velocity.— Fig. 5a-d shows velocities measured over the berm. In (a), the incident wave approaches the wall with quite uniform and horizontal velocities under its crest. In (b), velocities start converging, and slightly increasing at the front face. In (c), the jet starts forming close to the wall, with vertical velocities larger than horizontal ones. From (c) to (d), a "flip through" motion occurs at the wall, i.e., the wave front face rotates, forward of a free surface point of approximate coordinates (5.23,0.42), and this upward motion has quite a large acceleration. These successive stages are also observed in calculations (Fig. 3). Maximum measured acceleration of the waterline at the wall is $12g$, and its maximum measured velocity is $3\sqrt{gd}$. Both of these occur close to stage (d). These are quite smaller, however, than the extrema found in the calculations.

Instantaneous pressure on the wall.— Figure 6 shows measured pressure at locations

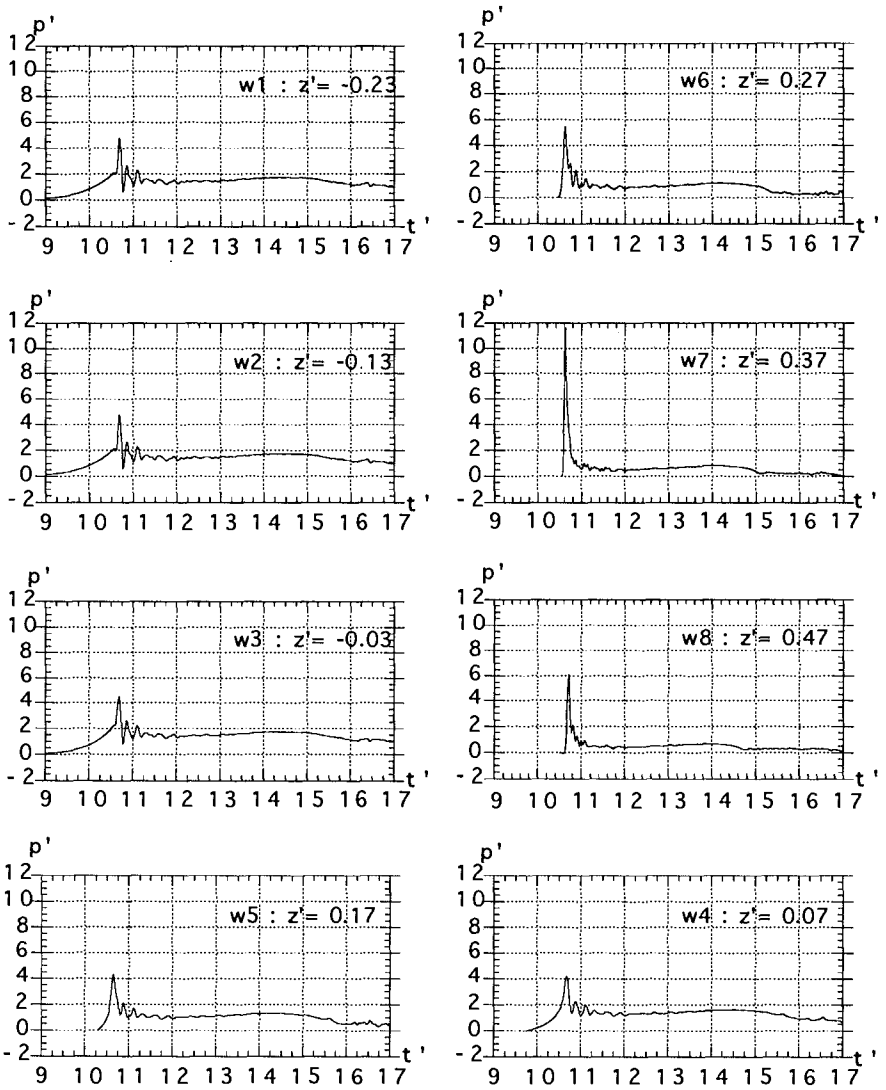

Figure 6: Pressure on the wall $p'(t')$, at $x' = 5.69$, as a function of z'.

(w1-w8) along the wall (Fig. 3). Dashes denote pressures that have been divided by the maximum pressure in still water, $p_H = \rho g d$. All pressure diagrams exhibit a peak of different magnitude, around time $t' = 10.65$ (versus 10.70 in computations). This means, local pressures almost simultaneously reach their maximum, and the envelope of maximum pressure can be used to calculate the maximum impact force on the wall. This was also observed by KIR.

Maximum peak pressure is $p'_{max} \simeq 12$, at gage w7, i.e., at $z' = 0.37$ above SWL. Peak pressure decreases both for larger and smaller values of z', but stays quite constant under SWL, down to the bottom. All peak pressures are followed by small high frequency oscillations. Structural vibrations of the vertical wall model have been eliminated by using a stiff thick plate, and stiffeners. Thus, high frequency oscillations can be a sign, a small quantity of air is imprisoned between the wave and the wall during the impact. Based on pressure diagrams in Fig. 6, however, air entrainment seems to be quite minor.

Instantaneous pressure on the berm.— Figure 7 shows measured pressure at locations (b1-b8) on the berm (Fig. 3). All pressure diagrams exhibit a peak of decreasing magnitude when x' decreases, i.e., when moving away from the wall. Peak pressure is reached at, or close to $t' = 10.65$, for all locations. All peak pressures again are followed by small high frequency oscillations. Maximum peak pressure is $p'_{max} \simeq 3.7$, at $x' = 5.62$, i.e., very close to the wall.

Although it had been suggested earlier that peak pressures might be large on the bottom, it is, to our knowledge, the first time, comprehensive measurements of wave pressure on the berm of a breakwater have been made. The large impact pressures on the bottom, as far away as $2.4d$, require that they be considered when analyzing the berm stability, particularly for porous berms with large permeability (coarse granular media), in which significant pore pressures can transmit, and uplift isolated armour blocks. This is obviously a point for further study.

Maximum pressure and force on the wall.— Figure 8 shows instantaneous computed pressure distributions on the wall, for the same times as successive water profiles in Fig. 3 (solid lines). Symbols in Fig. 8 represent maximum pressure measured at each location, (w1-w9), during 9 repetitions of the experiment.

Results show, maximum computed and measured pressures reach 24 and 12 times p_H, respectively, and large pressures also occur down to the toe of the wall (as expected from Fig. 6 and 7 and discussion above). Maximum pressure is located above SWL, at $z' = 0.39$ and 0.37, in the computations and in the experiments, respectively. At these locations, the pressure increases from zero up to the maximum over $\simeq 0.10$ time units. This can be seen from Fig. 6 for the experiments. Computed hydrostatic pressure is, $\rho g(\eta - z) = 0.36 p_H$, at $z' = 0.39$, i.e., 1/66 p'_{max}. Global shape of the pressure diagram is well predicted in the numerical model. Maximum pressure, however, is overpredicted in the model. This could be due to the following few reasons : (i) the incident wave is about 15% smaller in the experiments, due to

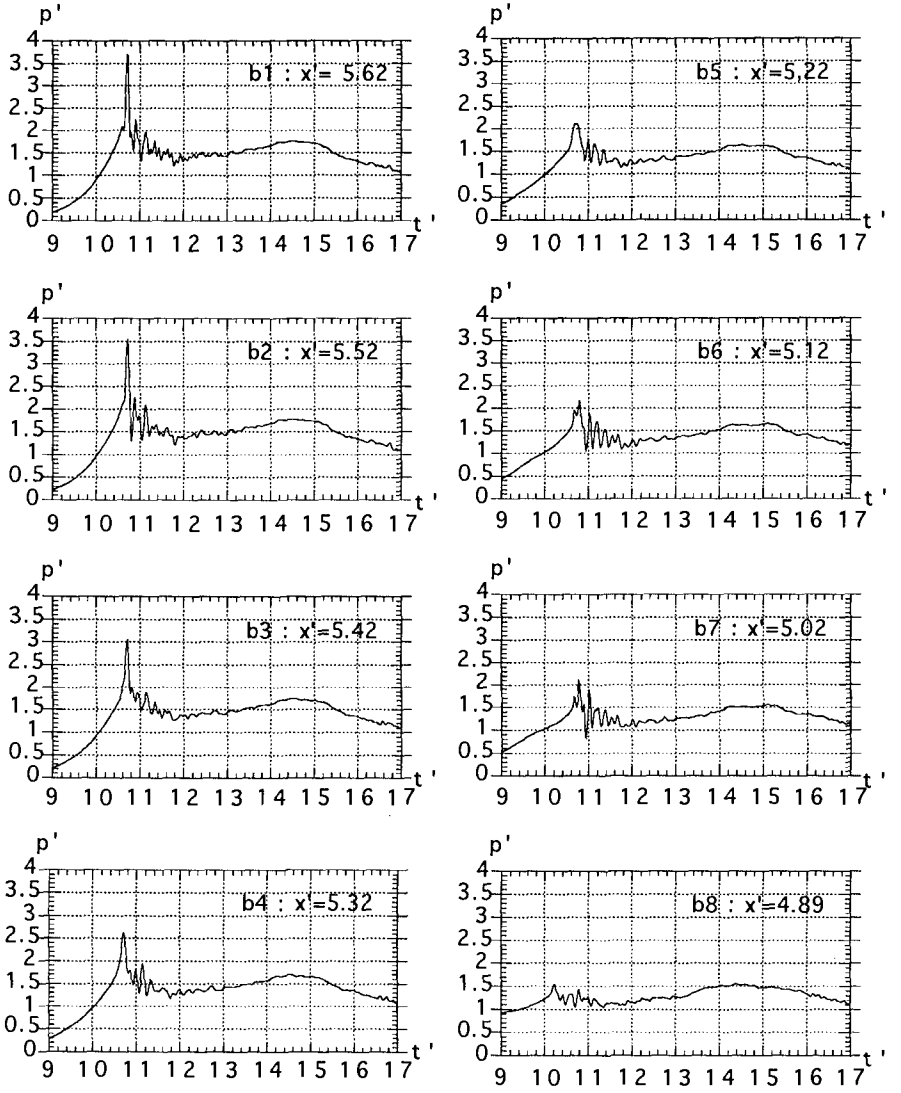

Figure 7: Pressure on the berm, $p'(t')$, at $z' = -0.33$, as a function of x'.

energy loss at the step. This leads to smaller impact pressures in the experiments; (ii) actual maximum pressures may have been "missed" in the measurements due to their very short time duration, and due to the size and location of pressure gages. The large dispersion of the measured pressure for $z' > 0$ in nearly identical repetitions of experiments, tends to support this hypothesis; (iii) the roughness of the wall and of the free surface may limit the intensity of the jet formation in the experiments (i.e., accelerations and velocities) and, thereby, the magnitude of the maximum pressure (as suggested by CP). This is supported by the relatively low acceleration and velocity measured for the waterline along the wall in the experiments (see above).

As discussed above, maximum pressure envelope should be almost identical to instantaneous maximum pressure diagram (last solid profile in Fig. 8). Hence, it can be used for calculating maximum impact force. Figure 9 shows the instantaneous pressure force on the wall, F'_x (scaled by $\frac{1}{2}p_H d$) as a function of time, in both experiments (solid line) and computations (chained line, up to maximum impact). The experimental force is simply based on integrating pressure diagrams in Fig. 6. Results show, numerical and experimental results quite well agree up to maximum impact. Computations, however, as could be expected from the pressures, overpredict maximum force.

As far as stability of the wall is concerned, Fig. 10 shows the time variation of computed force on the wall F'_x, and moment with respect to the toe of the wall M'_b (scaled $\frac{1}{6}p_H d^2$), up to $t' = 10.69$. These are compared to hydrostatic force F'_{Hx} and corresponding moment M'_{Hb}, based on wave elevation η at the wall. Last force and moment shown on the figure are about 3 and 5 times larger than corresponding hydrostatic values, respectively. Peak impact pressures were obtained for a slightly later time, $t' = 10.70$, for which $F'_x = 58.1$ and $M'_{Hb} = 245.5$, i.e. 9 and 15 times hydrostatic values, respectively.

Conclusions

Present experimental and numerical results are bringing new light into the creation of large wave impact pressures on a vertical wall. Peak pressures on the wall have clearly been linked to a converging flow, and to the formation of a small scale jet, with large vertical velocity and acceleration. Large impact pressures have also been measured and calculated on the berm, as far away as twice the local depth from the wall. Such pressures might be of importance for the stability of porous berms. Water compressibility and air entrainment do not seem to be important factors in the present case. Computational results are well supported by experiments.

Based on these results, the numerical model can now be used for predicting wave pressure forces on breakwaters of various geometric configurations, keeping in mind the limitations of potential flow theory. Later studies will include : sensitivity analysis of impact pressure to the geometry (e.g., effect of streamlining); design implication for the sliding and overturning stability of the vertical wall, under wave impact pressure (a method based on wave impulse is being considered).

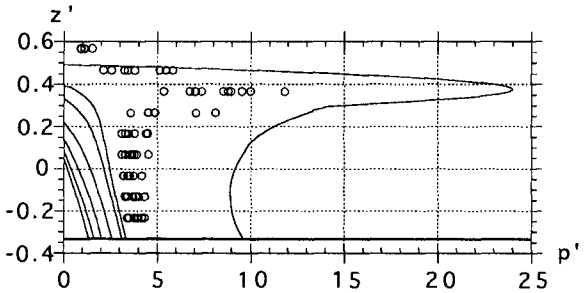

Figure 8: Impact pressure on the wall : (o) $p'_{max}(z')$ in nine repetitions of experiments; (—) computed pressure $p'(z')$ for surface profiles of Fig. 3.

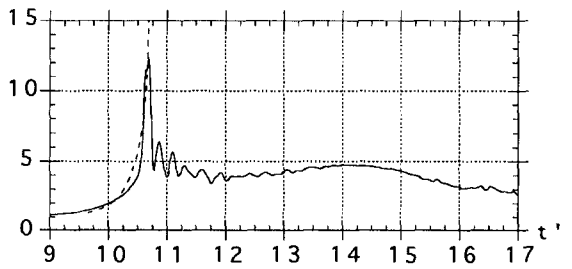

Figure 9: Impact force on the wall, $F'_x(t')$: (—) experiments; (- - -) computations.

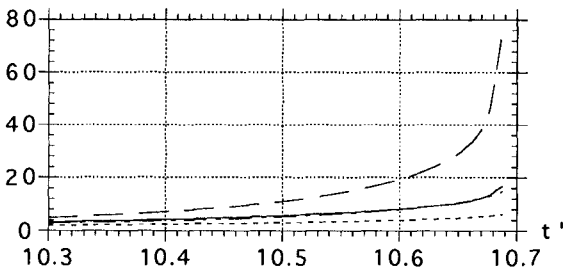

Figure 10: Computed impact force and moment on the wall : (———) F'_x total force; (- - - -)F'_{Hx} hydrostatic force based on η at the wall; (— —) M'_b total moment with respect to bottom; (– – –) M'_{Hb} total hydrostatic moment.

Acknowledgments

The authors acknowledge financial support from the "NATO Research Grant No. CRG-901019", and the first author from the "NSF Grant No. BCS-9111827".

References

Cooker, M. and Peregrine, D.H. (1991) "Violent Water Motion at Breaking-Wave Impact." In *Proc. 22nd Intl. Conf. on Coastal Engineering* (ICCE22, Delft, The Netherland, July 90) Vol.**1**, 164-176, ASCE.

Dold, J.W. & Peregrine, D.H. (1986) "An Efficient Boundary Integral Method for Steep Unsteady water Waves." *Numerical methods for Fluid Dynamics II* (ed. K.W. Morton & M.J. Baines), pp. 671-679. Clarendon Press, Oxford.

Goda, Y. (1985). *Random Seas and Design of Maritime Structures.* Univ. of Tokyo Press.

Führböter, A. (1985) "Model and Prototype Tests for Wave Impact and Run-up on a Uniform 1:4 Slope." *Coastal Engng.* **10** 49-84.

Goring D.G. (1978) "Tsunamis - The Propagation of Long Waves onto a Shelf." *W.M. Keck Laboratory of Hydraulics and Water Resources, California Institute of Technology, Report No.* **KH-R-38.**

Grilli, S, Losada, M.A. and Martin, F. (1992) "The Breaking of Solitary Waves over a Step : Modeling and Experiments" In *Proc. 4th Intl. Conf. on Hydraulic Engineering Software* (HYDROSOFT92, Valencia, Spain, July 92) (eds. W.R. Blain and E. Cabrera), Fluid Flow Modelling, pp. 575-586. CMP & Elsevier Applied Science.

Grilli, S., Skourup, J. & Svendsen, I.A. (1989) "An Efficient Boundary Element Method for Nonlinear Water Waves." *Engineering Analysis with Boundary Elements,* **6** (2), 97-107.

Grilli, S. & Svendsen, I.A. (1990) "Corner Problems and Global Accuracy in the Boundary Element Solution of Nonlinear Wave Flows." *Engineering Analysis with Boundary Elements* **7** (4), 178-195.

Grilli, S. and Svendsen, I.A. (1991a) "Wave Interaction with Steeply Sloping Structures." In *Proc. 22nd Intl. Conf. on Coastal Engineering* (ICCE22, Delft, The Netherland, July 90) Vol. **2**, pps. 1200-1213, ASCE edition.

Grilli, S. and Svendsen, I.A. (1991b) "The Propagation and Runup of Solitary Waves on Steep Slopes." *CACR, University of Delaware, Research Report* **91-4.**

Kirkgöz, M.S. (1982) "Shock Pressure of Breaking Waves on Vertical Walls." *J. Waterway, Port, Coastal, and Ocean Engng.* **108,** 81-95.

Kirkgöz, M.S. (1991) "Impact Pressure of Breaking Waves on Vertical and Sloping Walls." *Ocean Engng.* **18** (1/2), 45-59.

Losada, M.A., Vidal, C. and Medina, R. (1989) "Experimental Study of the Evolution of a Solitary Wave at an Abrupt Junction." *J. Geophys. Res.* **94** (C10), 14557-14566.

Partenscky, H.-W. (1988) "Dynamic Forces Due to Wave Breaking at Vertical Coastal Structures." In *Proc. 2nd. Intl. Work. Coastal Zones,* pp. 4.1-4.15. Tech. Univ. of Athens.

Wang, Y.X. & Su, T.C. (1992) "Numerical Simulation of Breaking Waves Against Vertical Wall." In *Proc. Offshore and Polar Engng. Conf.* (ISOPE92, San Francisco, June 92) .